ISSN (Print) 1226-1750
ISSN (Online) 2233-6656
**Journal of Magnetics** 20(3), 308-311 (2015) http://dx.doi.org/10.4283/JMAG.2015.20.3.308

# Design of Crisscrossed Double-Layer Birdcage Coil for Improving $B_1^+$ Field Homogeneity for Small-Animal Magnetic Resonance Imaging at 300 MHz

**Jeung-Hoon Seo, Sang-Doc Han, and Kyoung-Nam Kim***

*Center for Molecular and Cellular Imaging, Samsung Biomedical Research Institute, Seoul 135-710, Korea*

(Received 12 May 2015, Received in final form 22 June 2015, Accepted 25 June 2015)

**We design a crisscrossed double-layer birdcage (DLBC) coil by modifying the coil geometry of a standard single-layer BC (SLBC) coil to enhance the homogeneity of transmitting magnetic flux density ($B_1^+$) along the main magnetic field ($B_0$)-direction for small-animal magnetic resonance imaging (MRI) at 300 MHz. The performance assessment of the crisscrossed DLBC coil is conducted by computational analysis with the finite-difference time domain method (FDTD) and compared with SLBC coil in terms of the $B_1$ and the $B_1^+$ distribution. As per the computational calculation studies, the mean value in the two-dimensional $B_1^+$ map obtained at the mid-axial slice with the proposed DLBC coil is slightly lower than that obtained with the SLBC coil, but the $B_1^+$ value of the DLBC coil in the outermost plane (40 mm away from the central plane) shows improvements of 19.3% and 24.8% over the SLBC coil $B_1^+$ value when simulating a spherical phantom and realistic mouse body modeling. These simulation results indicate that, the $B_1^+$ homogeneity along the z-direction was improved by using DLBC configuration. Our approach enables $B_1^+$ homogeneity improvement along the z-direction, and it can also be applied to ultra-high field (UHF) MRI systems.**

**Keywords :** magnetic resonance imaging, double-layer, single-layer, birdcage coil, $B_1$ field in-homogeneity

## 1. Introduction

Ultra-high field (UHF) strengths ($\geq$ 7.0 T) and high performance of radiofrequency (RF) coils are crucial to small-animal magnetic resonance imaging (MRI) systems to obtain high-resolution anatomical imaging [1, 2]. HF MRI scanner have found use in a wide range of medical applications from neuroimaging to oncological investigations for the image quality they provide [3-5]. In this backdrop, researchers have designed and developed various geometries of the RF coil that provides the excitation pulse for generating the transmitting ($B_1^+$) field and highly sensitive receiving fields ($B_1^-$) for the MR signals emitted from the imaged subject [6, 7].

The birdcage (BC) RF volume coil is commonly used for volumetric anatomy. In order to achieve both higher frequencies and a closer approximation to the ideal cosine distribution, volume-coil-based BC designs have focused on using a large number of legs [8]. The BC coil is commonly used in the transmit/receive (Tx/Rx) and Tx-only configurations. In particular, the Tx-only BC coil that consists of the phased array coil has long been considered the clinical workhorse at field strengths of 1.5 T and 3.0 T [9-11]. However, in higher-frequency environments, the superimposed RF wave behavior at high Larmor frequencies corresponding to small RF wavelengths yields an inhomogeneous $B_1^+$ distribution along the main magnetic field ($B_0$) direction regardless of the utilization of the BC coil [12, 13]. The $B_1^+$ in-homogeneity becomes increasingly severe at high Larmor frequencies, and this inhomogeneous $B_1^+$ field can adversely affect the flip angle in tissues. Therefore, addressing the $B_1^+$ in-homogeneity forms an important aspect of BC coil design [14].

In this study, we propose a crisscrossed double-layer BC (DLBC) coil, which consists of the standard single-layer birdcage (SLBC) coil with an additional layer wound in the form of a crisscrossed loop, to improve the $B_1^+$ field homogeneity along the $B_0$ direction (i.e., the z-direction) under a field of 7 T at 300 MHz. The DLBC coil performance is compared with that of the standard SLBC coil in terms of the $B_1^+$ homogeneity. The numerical calculations for the DLBC coil are performed by using the finite-difference time domain method (FDTD) on a spherical phantom and a realistic mouse body model.


*Corresponding author: Tel: +82-32-460-9015
Fax: +82-2-3410-3628, e-mail: kn76.kim@hotmail.com

## 2. Material and Methods

Figure 1 shows the standard 8-leg SLBC and our DLBC coil modeled via FDTD in order to compare their performances in terms of the $B_1^+$ field homogeneity. The modeled SLBC coil (Fig. 1(a)) does not include any additional layer. On the other hand, our DLBC coil design uses crisscrossed looping of an additional layer (Fig. 1(b)). The width of the additional layer in the secondary triangular coil (Ws) is 19 mm, and the points of intersection of the layer with the end-ring of the BC are 4 mm away from the closest standard BC-coil-leg position. The length of the secondary coil (Ls) along the vertical direction of the BC is 47 mm. Each BC coil has a diameter of 72 mm and length of 100 mm. The RF shield is assigned as a perfect electric conductor (PEC) with modeling dimensions of 110-mm diameter and 100-mm length, and it is positioned in the outer region of the BC coil.

In the study, the loading conditions corresponding to the spherical phantom and the realistic mouse body model were numerically simulated at a field of 7 T and frequency of 300 MHz. Two loading structures were positioned in the inner region of each BC coil. The permittivity and conductivity of the spherical phantom were set as $\varepsilon_r = 59$ and 0.5 S/m, respectively. These values are crucial to understand the RF wave behavior arising from the interactions between the coil and subject. With regards to the mouse body model, 18 tissue types (e.g., blood, cartilage, cerebellum, cerebrospinal fluid (CSF), dura, white matter (WM), gray matter (GM), etc.) were simultaneously simulated. The electrical tuning capacitance ($C_T$) was replaced by a current source in the simulation, and it was placed in the end-ring of the coil as per the BC configuration. By different types of the filter, it can be categorized into high-pass filter (HPF), low-pass (LPF), and band-pass filter (BPF). The generally used HPF BC coil was chosen due to the high B1 field strength in the central region of the coil. The calculated FDTD results were reconstructed for a quantitative comparison of the $B_1^+$ distribution by using Matlab (Version 7.1, Mathworks Inc., Matick, MA, USA). The normalization of the $B_1^+$ map with the value of 2 μT was performed at the isocenter of each BC coil [15].

## 3. Results and Discussion

Figure 2 shows the distributions of the $B_1$ field including the $B_1^+$ component in the mid-sagittal (x–z) plane and the signal intensity (SI) profiles for the SLBC and DLBC coils. The SLBC coil exhibits a centrally focused $B_1$ distribution, and its SI gradually decreases in the peripheral regions due to the standing RF wave effect under high-frequency operation. The observed difference in the $B_1$ field distribution between the two BC coils is due to the presence of the additional layer in the DLBC coil. The DLBC coil with its additional layer supplements the weak signal in the end-ring region along the z-direction of the coil. The proposed coil configuration is similar to Litzcage coil, which is inserting an insulated crossover at the center of each rungs of SLBC coil [16]. For a more detailed investigation, we compared the one-dimensional SI curves of the SLBC and DLBC coils (along the line $P_1$-$P_2$ in Figs. 2i and 2ii) along the z-direction in the spherical phantom. The SLBC SI profile exhibits a convex-shaped curve. The difference between the maximum and minimum $B_1$ field strengths is 11.5% (1.957/1.755). In contrast, the DLBC SI profile exhibits increased $B_1$ field homogeneity along the z-direction with respect to that obtained with the SLBC coil. Consequently, the DLBC-coil $B_1$ field variance is as small as 2.9% (1.983/1.926).

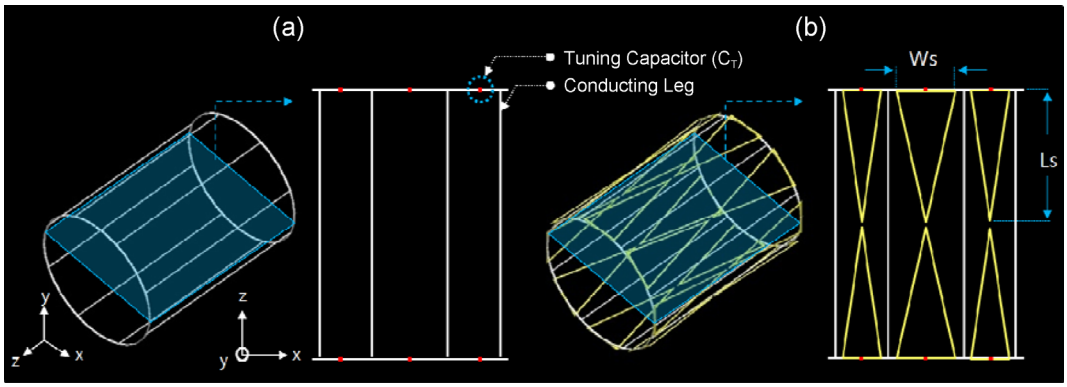


**Fig. 1.** (Color online) (a) Standard single-layer birdcage (SLBC) and crisscrossed double-layer birdcage (DLBC) coil modeled using finite-difference time domain (FDTD) calculations. The BC coils have a diameter of 72 mm and length of 100 mm. The width of the secondary coil (Ws) is 19 mm, and the distance between the coil edge (where it meets the end-ring) and the leg is 4 mm on either side. The length of the secondary coil (Ls) is 47 mm.

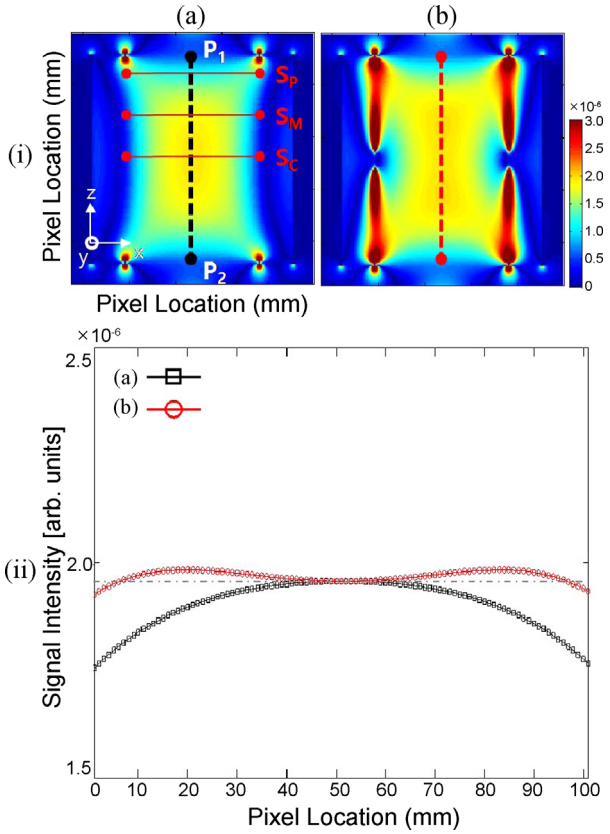


**Fig. 2.** (Color online) (i) $B_1$ field distributions in the mid-sagittal (x–z) plane and (ii) signal intensity (SI) profiles along $P_1$-$P_2$ for (a) single-layer birdcage (SLBC) and (b) double-layer birdcage (DLBC).

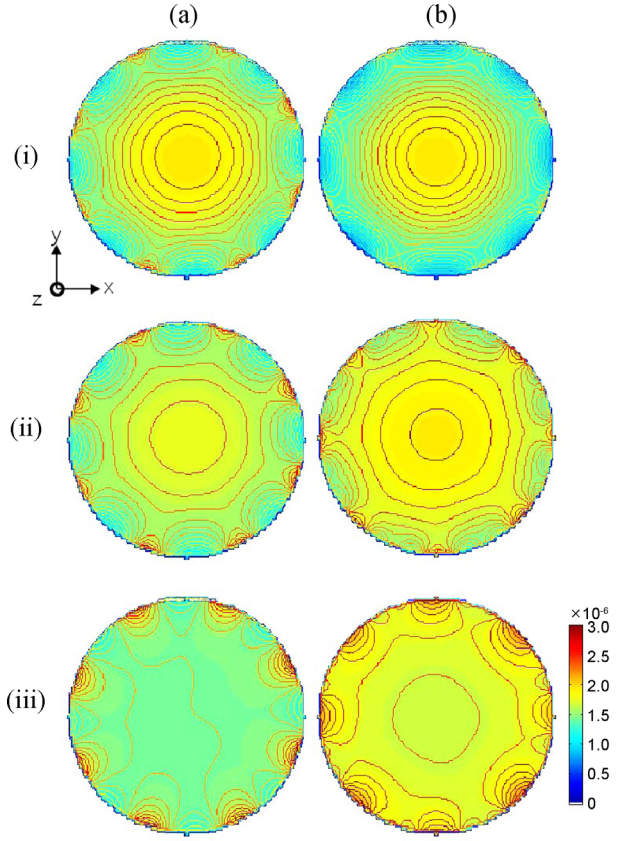


**Fig. 3.** (Color online) $B_1^+$ distributions of (a) single-layer birdcage (SLBC) and (b) double-layer birdcage (DLBC) coils in terms of contour and color map at three positions: (i) mid-transversal slice (plane $S_C$ in Fig. 2) and (ii) 20 mm (plane $S_M$ in Fig. 2) and (iii) 40 mm (plane $S_P$ in Fig. 2) from the mid-transversal slice.

These results indicate that the DLBC coil provides superior $B_1$ homogeneity than the SLBC coil.

Figure 3 shows the $B_1^+$ distribution in terms of the contour and color map at the mid-axial slice (Fig. 3i, corresponding to plane $S_C$ in Fig. 2) and at distances of 20 mm (Fig. 3ii, corresponding to plane $S_M$ in Fig. 2) and 40 mm (Fig. 3iii, corresponding to plane $S_P$ in Fig. 2) away from the mid-axial slice. As regards the mid-axial-slice $B_1^+$ field distribution, both BC coils exhibit similar field distributions. The $B_1^+$ in-homogeneity is observed for both BC coils away from the central region. However, DLBC-coil $B_1^+$ field homogeneity is relatively higher than that of the SLBC coil. The mean $B_1^+$ values mapped at three different slice positions (peripheral slice or $S_P$, mid-slice or $S_M$, and central slice $S_C$) for the phantom are listed in Table 1a. The mean $B_1^+$ value at $S_C$ for the SLBC coil is 7% (1.570/1.473) higher than that at the $S_C$ position for the DLBC coil; however, the mean $B_1^+$ values in the case of the SLBC coil at $S_M$ and $S_P$ decrease by 11.2% (1.737/1.562) and 19.3% (1.758/1.473), respectively, in comparison with the corresponding $B_1^+$ values in the case of the DLBC. Although SLBC-coil $B_1^+$ field intensity is greater than that of the DLBC in the central region, field homogeneity in the outer region decreases when compared to that for the DLBC coil.

Figure 4 compares the $B_1$ field distributions of the standard SLBC coil (Fig. 4(a)) and the proposed DLBC coil (Fig. 4(b)) for the mouse body model. The original mouse body model was reduced by 55% of its original size. The proposed DLBC coil and the standard SLBC coil exhibit similar color distributions, which similarity indicates a homogeneously distributed $B_1^+$ field in both cases. However, the mean $B_1^+$ values at the two peripheral-slice positions ($S_{P1}$ and $S_{P2}$) in the case of the DLBC coil are close to the mean $B_1^+$ value in the central region. The mean-$B_1^+$-value differences between the central region and the two peripheral regions are 1.5% (1.876/1.847) and 1.9% (1.883/1.847) for the DLBC coil, as listed in Table 1b. Thus, the results of our study indicate that the standard SLBC coil exhibits a large $B_1^+$ in-homogeneity

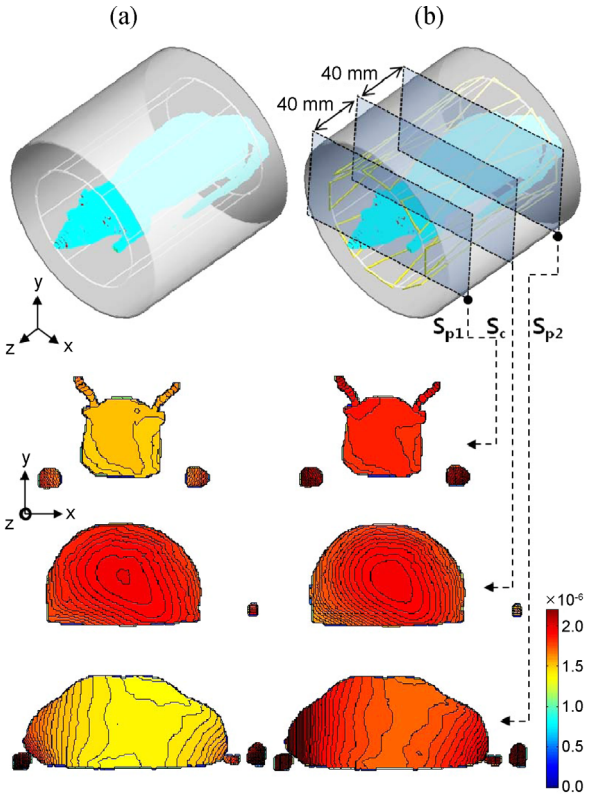


**Fig. 4.** (Color online) $B_1^+$ distributions of (a) single-layer birdcage (SLBC) coil and (b) double-layer birdcage (DLBC) coil for realistic mouse body model.

**Table 1.** Mean $B_1^+$ values at three slice locations: three different slices for single-layer birdcage (SLBC) and double-layer birdcage (DLBC) coils for cases of spherical phantom and mouse body model.

| | Slice Position | SLBC | DLBC |
|---|---|---|---|
| (a) Phantom | $S_C$ | 1.570 | 1.473 |
| | $S_M$ | 1.562 | 1.737 |
| | $S_P$ | 1.473 | 1.758 |
| (b) Mouse | $S_{P1}$ | 1.503 | 1.876 |
| | $S_C$ | 1.885 | 1.847 |
| | $S_{P2}$ | 1.557 | 1.883 |

field distribution along the z-direction, and this in-homogeneity is largely mitigated with the use of our proposed DLBC coil.

## 4. Conclusion

The use of the standard BC coil in small-animal MRI does not fully address the $B_1^+$ in-homogeneity problem. Thus, we proposed a DLBC coil with a crisscrossed additional layer, and we compared its performance with that of the SLBC coil. The proposed DLBC coil provides better $B_1^+$ field homogeneity along the z-direction, and thus, it is highly suitable for providing a homogeneous magnetic flux ($B_1$) radiation across a large volume at 7 T.

## Acknowledgment

This study was supported by a Samsung Biomedical Research Institute grant (SMX1132851).

## References

[1] F. Schick, Eur. Radiol. **15**, 946 (2005).
[2] P. Marzola, F. Osculati, and A. Sbarbati, Eur. Radiol. **48**, 165 (2003).
[3] A. Hahn, G. S. Kranz, E. M. Seidel, R. Sladky, C. Kraus, M. Küblböck, D. M. Pfabigan, A. Hummer, A. Grahl, S. Ganger, C. Windischberger, C. Lamm, and R. Lanzenberger, NeuroImage **82**, 336 (2013).
[4] L. Huber, J. Goense, A. J. Kennerley, R. Trampel, M. Guidi, E. Reimer, D. Ivanov, N. Neef, C. J. Gauthier, R. Turner, and H. E. Möller, NeuroImage **107**, 22 (2015).
[5] S. Francis and R. S. Panchuelo, Physiol. Meas. **35**, 167 (2014).
[6] I. Connell, K. Gilbert, M. Abou-Khousa, and R. Menon, IEEE. Trans. Med. Imaging. **34**, 825 (2015).
[7] J. Moore, M. Jankiewicz, H. Zeng, A. W. Anderson, and J. C. Gore, J. Magn. Reson. **205**, 50 (2010).
[8] M. Joël, M. Lupu, and B. Andre, NMR Probeheads for Biophysical and Biomedical Experiments, Imperial College Press, London, (2006) pp. 374.
[9] C. E. Hayes, W. A. Edelstein, J. F. Schenck, O. M. Mueller, M. Eash, J. Magn. Reson. **63**, 622 (1985).
[10] M. Alecci, C. M. Collins, M. B. Smith, and P. Jezzard, Magn. Reson. Med. **46**, 379 (2001).
[11] R. Mekle, W. van der Zwaag, A. Joosten, and R. Gruetter, MAGMA. **21**, 53 (2008).
[12] S. Josan, Y. F. Yen, A. Pfefferbaum, D. Spielman, and D. Mayer, J. Magn. Reson. **209**, 332 (2011).
[13] T. S. Ibrahim, R. Lee, B. A. Baertlein, and P. M. Robitaille, Phys. Med. Biol. **46**, 609 (2001).
[14] K. Sung, B. L. Daniel, and B. A. Hargreaves, J. Magn. Reson. Imaging. **38**, 454 (2013).
[15] C. M. Collins, S. Li, and M. B. Smith, Magn. Reson. Med. **40**, 847 (1998).
[16] F. D. Doty, G. Entzminger, J. Kulkarni, K. Pamarthy, and J. P. Staab, NMR Biomed. **20**, 304 (2007).